Korean J. Chem. Eng., 40(7), 1775-1782 (2023)
DOI: 10.1007/s11814-023-1409-z

pISSN: 0256-1115
eISSN: 1975-7220

Membraneless enzymatic biofuel cells using three-dimensional graphite felt electrodes

Joonyoung Lee*, Kyuhwan Hyun*,, and Yongchai Kwon*,**,***,†**

*Department of Chemical and Biomolecular Engineering, Seoul National University of Science and Technology, 232 Gongneung-ro, Nowon-gu, Seoul 01811, Korea
**Energy & Environment Research Institute, Seoul National University of Science and Technology, 232 Gongneung-ro, Nowon-gu, Seoul 01811, Korea
***Department of Energy and Chemical Engineering, Seoul National University of Science and Technology, 232, Gongneung-ro, Nowon-gu, Seoul 01811, Korea
(*Received 17 January 2023 • Revised 14 February 2023 • Accepted 28 February 2023*)

Abstract−Membraneless enzymatic biofuel cells (EBFCs) have the potential to be used in biocompatible devices, such as implantable or wearable devices. However, they face challenges due to low reaction surface area and high resistance attributed to large particle size and protein composition of enzyme catalysts used. In this study, to improve the performance of membraneless EBFCs, three-dimensional graphite felt (3D-GF) electrode was utilized. The 3D-GF electrode has high electrical conductivity and large surface area, allowing the large loading of catalytic components and increasing the reactivity of redox reaction required for EBFC operation. Membraneless EBFC using the 3D-GF electrode is prepared with anodic catalyst including glucose oxidase (GOx) and tetrathiafulvalene mediator, and cathodic catalyst of horseradish peroxidase and GOx. The outermost layer of 3D-GF electrode is coated with gelatin crosslinked by glutaraldehyde to prevent leaching of components of catalysts. According to evaluations, both anodic and cathodic catalysts are evenly distributed on 3D-GF electrode, and anodic and cathodic currents of 103.5 and 68.7 μA at 0.3 V vs. Ag/AgCl are measured. Additionally, EBFCs using the optimized electrodes demonstrate high power output of 82 μW in a small cell kit size of 1.5×1.5×1.5 cm^3, with excellent design flexibility.

Keywords: Membraneless Enzymatic Biofuel Cell, 3D Graphite Felt Electrode, Tetrathiafulvalene, Glucose Oxidase, Horseradish Peroxidase

INTRODUCTION

Excessive consumption of traditional fossil fuels causes environmental degradation due to greenhouse effect caused by CO_2 generation and the depletion of fossil fuel reserves. Thus, many studies have sought to find alternative renewable energy sources and systems. Among them, fuel cells can be a promising and viable technology that can continuously produce electrical energy without CO_2 generation. They use a mechanism that converts chemical energy originating from fuels into electrical energy through electrochemical redox reactions, while the amount of emitted CO_2 can be significantly reduced by using them [1,2]. Among them, enzymatic biofuel cells (EBFCs) can be used for implantable medical devices, such as insulin pumps, self-powered glucose sensors, pacemakers, cochlear implants, and deep brain stimulators [3-5].

In contrast to other types of fuel cells that use metal catalysts, EBFCs use enzymes as catalyst and are operated under mild conditions of room temperature and electrolytes of neutral pH [6,7]. Due to these unique benefits, EBFCs can be implanted into the human body [8]. Furthermore, since enzymes have strong substrate specificity, membrane is unnecessary, and thus, the design of flexible EBFC kit is possible [9]. Regarding fuels, EBFCs often use metabolites, such as glucose, sucrose, and fructose, which are produced renewably by biological metabolism [10,11]. With the metabolite fuels, the possibility of fuel depletion becomes lowered. Of the famous metabolites, there is glucose. When glucose is considered as fuel for EBFCs, glucose oxidase (GOx) is often used as enzyme catalyst because GOx can promote glucose oxidation reaction (GOR); that is one of main anodic reactions required for running EBFCs [12-14]. GOx comprises homodimer and redox active site, flavin adenine dinucleotide (FAD) cofactor. In addition, this is cheaper than other metal catalysts due to its easy and large productivity [15].

However, GOx cannot directly transfer the electrons produced by GOR to electrode due to a long distance between FAD cofactor that is deeply embedded within the outer shell of GOx and electrode [16]. Therefore, to activate GOR and transfer the electrons produced by GOR to electrode more conveniently, mediated electron transfer (MET) using mediator can be regarded. Here, the mediator facilitates electron transfer between FAD cofactor and electrode through its reversible redox reaction and relatively easy movement. As the mediator, ferrocene, dopamine, tetrathiafulvalene (TTF), quinone derivatives, and osmium redox polymer, have been used [17-21]. Among them, TTF is determined as a mediator for this study because this has excellent redox reactivity and negative onset potential for GOR [22]. Taken together, when GOx and TTF are involved in anode for GOR, the following reactions are expected.

$$\text{Glucose} \xrightarrow{GOx} \text{Gluconic acid} + 2H^+ + 2e \quad (1)$$

†To whom correspondence should be addressed.
E-mail: kwony@seoultech.ac.kr

$$GOx(FAD)+2H^{+}+2e\rightarrow GOx(FADH_2) \quad (2)$$

$$GOx(FADH_2)+2TTF^{+}\rightarrow GOx(FAD)+2H^{+}+2TTF \quad (3)$$

$$2TTF\rightarrow 2TTF^{+}+2e \quad (4)$$

As earlier explained, since GOx has a large particle size and its active site is in a deep pocket, the magnitude of power produced by EBFC operated using GOx is usually low. To increase the power produced by EBFC, it is important to increase the loading amount of components included in catalyst and the electron transfer and diffusion rates.

For these purposes, there have been some previous studies. In the approaches to increase the loading amount of catalyst including enzyme, Kwon group used hierarchically structured reduced graphene oxide (rGO) as the supporting material for immobilizing as many as possible catalyst components, while TTF was considered as mediator. As a result, the loading amount of enzyme molecules increased with the optimized structure, while their redox reactivity and current were also improved [23]. In the approaches to promote electron transfer and diffusion rates, Yuanjing et al. improved ion diffusion and interaction by forming a nanoporous membrane binder structure using NiHCF and agarose [24].

In contrast to the anodic catalyst promoting GOR, laccase and bilirubin oxidase are enzymes for cathode because they can effectively facilitate oxygen reduction reaction (ORR) [25-27]. However, different from GOx, they use direct electron transfer (DET) mechanism because cofactors included within them are located on their outer layer and, thus, the enzymes do not need to use a mediator for electron transfer [28,29]. Despite that, the two enzymes contain copper (Cu) atoms in their cofactors that are less active when they meet chloride or urate contained in body fluids and, thus, alternative ways to mitigate the issue are required [30]. To do that, cascade reaction can be suggested [31-33]. For this reaction, a sequential allocation of two enzymes consisting of GOx and hydrogen peroxidase (HRP) is recommended. In this cascade structure, GOx promotes the reduction reaction of O_2 into H_2O_2 when glucose is oxidized under O_2 state. Then such generated H_2O_2 is further reduced into H_2O by HRP. The entire reactions are as follows.

$$Glucose+O_2 \xrightarrow{GOx} Gluconic\ acid+H_2O_2 \quad (5)$$

$$H_2O_2+2H^{+}+2e \xrightarrow{HRP} 2H_2O \quad (6)$$

HRP is an enzyme that receives electrons directly from electrode and reduces H_2O_2 to H_2O. Therefore, several groups have suggested the combinational structure of HRP and GOx as cathodic catalyst. For instance, Pinyou group used 1-pyrenebutyric acid N-hydroxysuccinimide ester (PBSE) to immobilize HRP to electrode, and Cosnier group wired GOx and HRP using 1-pyrene boronic acid [34,35]. In addition, Kwon group replaced HRP with hemin to prepare for cathodic catalyst with GOx [36].

However, in the previous studies, fuel cell tests were conducted in small electrodes of less than 1 cm^2, and thus, the tests did not show the performance data in actual scale-up situation. For example, for operating a pacemaker, power of 10-50 μW level is needed, but power produced from the previous studies was less than 10 μW, and such a low power range was not enough to operate the pacemaker [37,38].

In this study, a new approach to increase the loading amount of enzyme catalyst and promote electron transfer is suggested to alleviate the low power issue of EBFC. More specifically, we use a 3D electrode that replaces conventional 2D electrode, and due to the use of 3D electrode, as many as possible enzyme based catalyst molecules are loaded. In actual electrode structure, GOx and TTF are immobilized onto graphite felt (GF) electrode to promote GOR in anode, while multi wall carbon nanotube (MWCNT), HRP, and GOx are immobilized onto GF electrode to promote H_2O_2 reduction reaction (HPRR) in cathode. In addition, both electrodes use the gelatin crosslinked by glutaraldehyde (GA) as a binder. It was already reported that the leaching out of enzyme and mediator molecules immobilized on GF electrode was significantly reduced [22,23]. To characterize the performance of 3D electrode and EBFC using the electrode, electrochemical measurements using cyclic voltammogram (CV) mode are carried out, while scanning electron microscopy (SEM) analysis is used to estimate whether the components of catalysts included in 3D electrode are properly dispersed on electrodes.

EXPERIMENTAL

1. Materials

Graphitized multiwall carbon nanotubes (MWCNTs, with ~99% purity) were used, manufactured by US Research Nanomaterials, Inc. SGL graphite felt was used (SIGRACELL battery felts GFD 4.65 EA, denoted H-SGL, 4.6 mm thick, SGL carbon). Glucose oxidase from Aspergillus niger (GOx, Type X-S, 100,000-250,000 units/g), peroxidase from horseradish (HRP, Type VI, ≥250 units/mg solid), gelatin from porcine skin (Type A, BioReagent, powder), glutaraldehyde solution (GA, grade II, 25% in water) were purchased from Sigma Aldrich. D-(+)-Glucose, anhydrous, 99%, was purchased from Alfa Aesar, and tetrathiafulvalene (TTF, >98.0%) was purchased from Tokyo Chemical Industry.

2. Preparation of Graphite Felt Electrode

To prepare for anode, 40 μL of 10 mM TTF solution dissolved in acetonitrile and 40 μL of 20 mg/mL GOx solution were drop cast onto GF electrode whose size was 1×1 cm^2, and the GF electrode including GOx solution was dried for 30 min. Such dried GF electrode was immersed in 5 wt% gelatin solution and dried for 1 h. After that, the GF electrode was dipped into 5 wt% GA solution for 1 min. The GF electrode including all the components was then washed with DIW and dried for 1 h. After that, GF/TTF/GOx/Gelatin-GA anode was prepared.

To prepare for cathode, GF electrode was immersed in 2.5 mg/mL MWCNT solution and shaken for one day. In turn, 40 μL of 40 mg/mL HRP solution and 40 μL of 20 mg/mL GOx solution were drop cast onto the GF electrode and, then, this was dried for 30 min [39]. GF electrode was then immersed in 5 wt% gelatin solution and dried for 1 h. The electrode was dipped into 5 wt% GA solution for 1 min. Following that, the GF electrode including all the components was washed with DIW and dried for 1 h. After that, the preparation of GF/HRP/GOx/Gelatin-GA cathode was done.

To optimize the loading amount of GOx in anode, the concen-

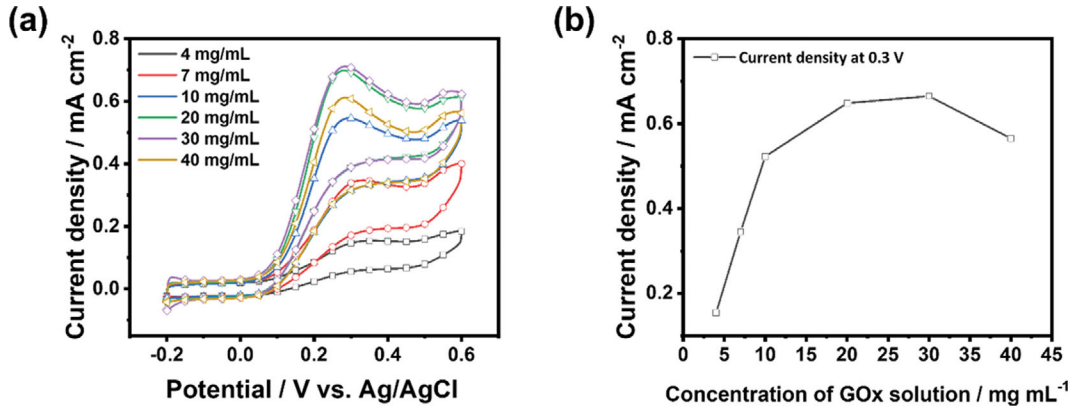

Fig. 1. (a) CV curves of GCE/CNT/TTF/GOx/Gelatin-GA showing the reactivity of GOR measured at different concentrations of GOx solution from 4 mg/mL to 40 mg/mL. For the tests, the applied potential range was −0.2-0.6 V vs. Ag/AgCl under 0.01 M PBS (pH 7.4) electrolyte with 100 mM glucose, and potential scan rate was 50 mV/s. (b) The current densities produced by GOR for the concentration variation of GOx solution. All the current densities were measured at 0.3 V vs. Ag/AgCl.

tration and volume of GOx solution should be well handled. Initially, an optimal concentration of GOx solution loaded onto glass carbon electrode (GCE) was determined. For doing that, the concentration of GOx contained in GCE/CNT/TTF/GOx/Gelatin-GA anode was gradually increased from 4 mg/mL to 40 mg/mL. By increasing the concentration, the current produced by GOR under 100 mM glucose and N_2 condition was measured (Fig. 1(a)). As shown in Fig. 1(a), the onset potential of GOR was 0.05 V vs. Ag/AgCl, while the effect of the concentration of GOx solution on the maximum current was summarized in Fig. 1(b). According to Fig. 1(b), when 20-30 mg/mL GOx solution was loaded, maximum current was 0.65-0.66 mA/cm^2. In contrast, when more than 40 mg/mL or less than 20 mg/mL GOx solution was loaded, the current rapidly decreased. With that, 20 mg/mL GOx solution was determined as an optimal concentration.

To optimize the volume of GOx solution through scale-up from GCE to GF electrodes, different volumes from 10 μL to 50 μL were drop cast onto GF electrode whose area was 1×1 cm^2. Here, when the volume of GOx solution increased to 40 μL, GF electrode absorbed the solution well. However, when than more than 50 μL GOx solution was loaded, GF electrode did not absorb the solution completely (see Fig. 2). Based on that, 40 μL was determined as an optimal volume of GOx solution. Through this, 40 μL of 20 mg/mL GOx solution was loaded for the preparation for anode.

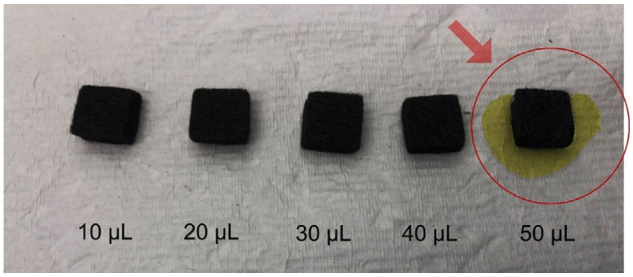

Fig. 2. Photo images showing the optimal volume of GOx solution onto GF electrodes. The volume of GOx solution was varied from 10 μL to 50 μL, and the solutions were drop cast onto GF electrode whose area was 1×1 cm^2.

3. Electrochemical and Optical Evaluations of the Catalysts

Cyclic voltammetry (CV) experiments were conducted in a three-electrode configuration using a Bio-Logic potentiostats, SP-240 electrochemical workstation (Bio-Logic, USA) linked to a personal computer. GF electrode was used as working electrode, while platinum wire and Ag/AgCl (sat. in 3.0 M NaCl) were considered counter and reference electrodes, respectively. All the tests were implemented under 0.1 M sodium acetate buffer solution (SAB, pH 5.2), and their potential scan rate was 10 mV/s. In-house PLA filament full cell kit was fabricated for measuring the performance of EBFCs and used to measure the polarization curve of each sample. For EBFC full cell tests, electrolyte consisted of 0.1 M glucose solution (0.1 M SAB, pH 5.2, air condition), and the EBFC full cell tests were carried out under 250 rpm.

High resolution-scanning electron microscope (HR-SEM, Hitachi SU8010, Japan) was used to investigate how the surface of electrodes was varied by sequential loading of enzyme and mediator molecules. The HR-SEM analysis was performed using 10.0 kV under a high vacuum and Pt coating. Energy dispersive X-ray spectrometer (EDS) has silicon drift diode 30 mm^2 active area detector type and 127 eV @ Mn standard peak resolution.

RESULTS AND DISCUSSION

1. Optical Analysis of 3D-GF Electrodes

This study aimed to load as many as possible enzyme and mediator molecules onto 3D-GF electrode to increase the power density of EBFC. For doing that, 3D-GF electrode structure with much larger active volume than 2D structure like GCE is proposed. The overall proposed structure of EBFC is presented in Scheme 1.

When electrode dimension is enlarged from 2D to 3D, one of the most important concerns is whether all the catalyst components can be evenly distributed inside the 3D electrode. To confirm that, cross-sectional images of 3D electrodes including all the catalyst components were examined by SEM, while all the components were identified by EDS analysis (Fig. 3). Regarding EDS analysis, it is initially expected that GOx, HRP, and gelatin will contain organic substances like C, N, and O, while S will be a main com-

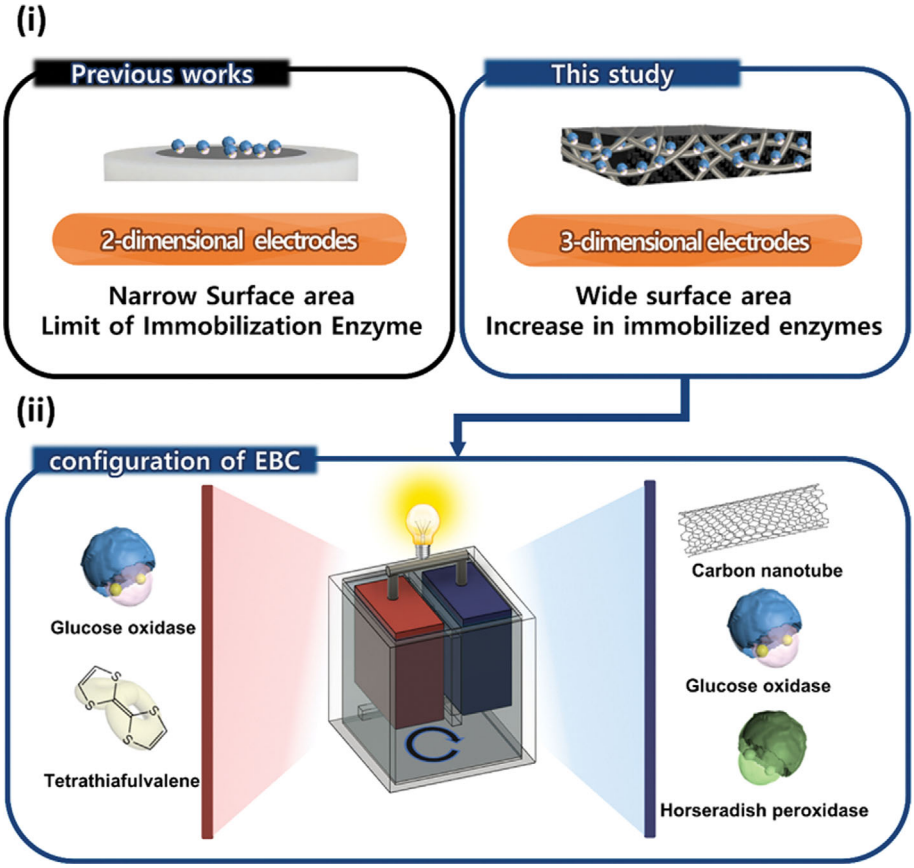

Scheme 1. Schematics showing (i) the difference in electrode structure between the conventional 2D electrode and a new 3D electrode studied in this work and (ii) overall EBC cell kit.

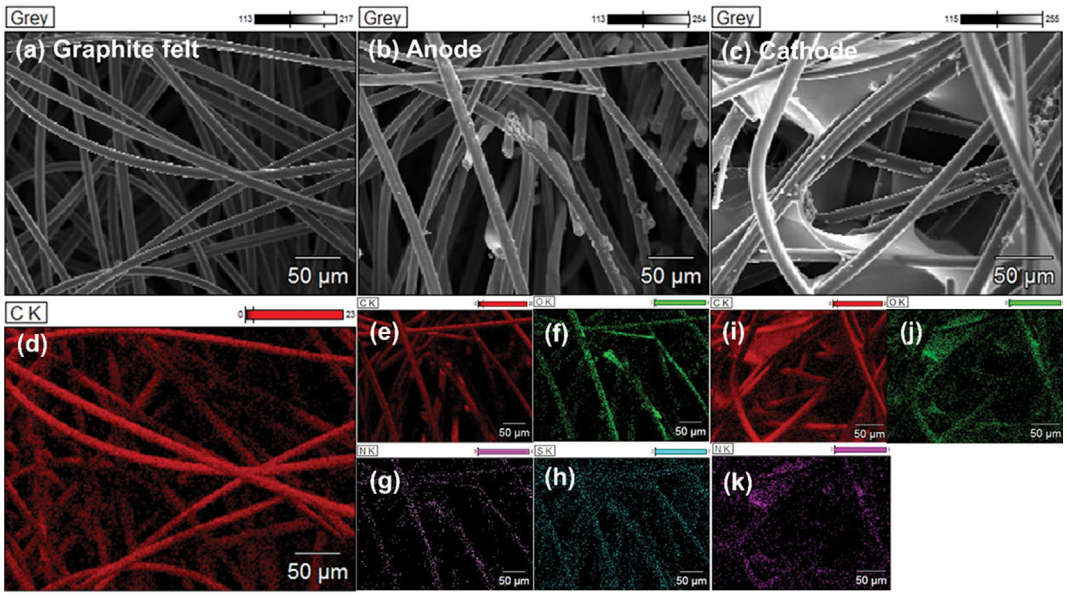

Fig. 3. SEM cross-sectional images of (a) pristine GF electrode, (b) anode, and (c) cathode. EDS mapping images of (d) carbon element contained in GF electrode, (e)-(h) carbon, oxygen, nitrogen, sulfur elements measured in anode, (i)-(k) carbon, oxygen, and nitrogen elements measured in cathode.

ponent of TTF. Thus, if 3D electrode is well fabricated, C, N, O, and S should be included in GF/TTF/GOx/Gelatin-GA anode, while C, N, and O should be included in GF/HRP/GOx/Gelatin-GA cathode. According to Fig. 3, C, N, O, and S were well recog-

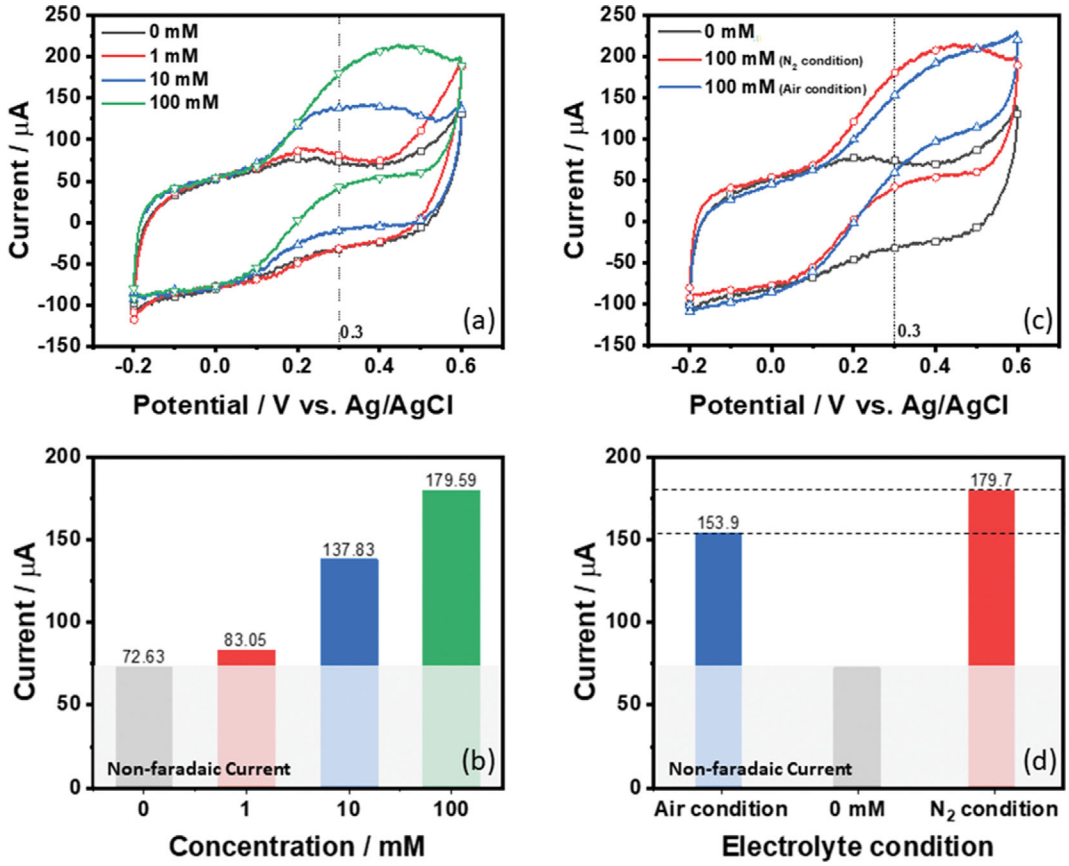

Fig. 4. (a) CV curves showing the reactivity of GOR measured by the injection of 0, 1, 10, and 100 mM glucose with GF/TTF/GOx/Gelatin-GA anode at N_2 state and (b) current densities showing the reactivity of GOR measured at 0.3 V vs. Ag/AgCl based on data of Fig. 4(a). (c) CV curves showing the reactivity of GOR measured by the injection of 0 and 100 mM glucose with GF/TTF/GOx/Gelatin-GA anode both at air and N_2 states based on data of Fig. 4(c). (d) current densities showing the reactivity of GOR measured at 0.3 V vs. Ag/AgCl.

nized in anode (Fig. 3(b)), while C, N, and O were well distributed in cathode without the observation of S (Fig. 3(c)). Based on that, this confirms that the components of both anodic and cathodic catalysts are well loaded on 3D-GF electrode.

2. Electrochemical Evaluations of Anode and Cathode

After GOR occurs at anode, two competitive reactions may occur. They are the oxidation reaction of ambient O_2 into H_2O_2 (reaction 5) and the redox reaction of TTF (reactions 3 and 4). Here, electrons produced by GOR can be used for both reactions, while TTF/GOx/gelatin-GA acts as anodic catalyst. Reactions 3 and 4 are desirable because these reactions can easily transfer electrons to electrode, whereas reaction 5 is a side reaction because this does not play a role in transferring electrons to electrode. Therefore, it is necessary to evaluate whether the desirable reactions (reactions 3 and 4) occur well with TTF/GOx/gelatin-GA catalyst even in ambient O_2 state. To investigate a proper pathway of the reactions, both O_2 and N_2 states (without O_2) were applied to electrolyte. In terms of glucose concentration that is provided to electrolyte, according to previous studies, when 100 mM glucose was provided as anodic fuel, EBFCs showed the best power performance. On the contrary, when the glucose concentration was more than 100 mM, this might interfere with mass transfer of glucose because the viscosity of electrolyte including glucose increased considerably. Therefore, 100 mM glucose was determined for this study [40].

The onset potential and current for GOR of GF/TTF/GOx/gelatin-GA anode are measured with sequential increase of glucose concentrations of 1, 10, and 100 mM under N_2 state (Fig. 4). In Fig. 4(a), the onset potential of GOR was close to 0.1 V vs. Ag/AgCl, while the current showing the reactivity of GOR was 5.9, 67.9, and 103.5 μA in the injection of 1, 10, and 100 mM glucose that were measured at 0.3 V vs. Ag/AgCl. Next, the reactivity of GOR was measured under air state with 100 mM glucose (Fig. 4(b)). As shown in Fig. 4(b), even in air state, the onset potential for GOR was 0.1 V vs. Ag/AgCl, while the current produced by GOR measured at 0.3 V vs. Ag/AgCl was 74.5 μA. Namely, the current produced by GOR in air state was 72% of that measured in N_2 state.

In contrast to anode, in GF/HRP/GOx/Gelatin-GA cathode, O_2 is reduced to H_2O_2 with the help of GOx (reaction 5), and then, such produced H_2O_2 is further reduced to H_2O with the help of HRP (reaction 6), which is called a cascade reaction. To evaluate the role of HRP in this cascade reaction, GF/HRP/Gelatin-GA cathode was fabricated without the loading of GOx, and its role was evaluated with the injection of H_2O_2 under air state. Here, the

concentrations of H_2O_2, 1, 3, and 5 mM are considered (Fig. 5). As shown in Fig. 5(a), when 1, 3, and 5 mM H_2O_2 were injected, their onset potential for HPRR was close to 0.8 V vs. Ag/AgCl, and the current showing reactivity of HPRR was 33.8, 76.6, 102.2 μA at 0.3 V vs. Ag/AgCl.

Next, cathodic cascade reaction was completed when GF/HRP/GOx/Gelatin-GA catalyst containing GOx molecules used glucose as fuel instead of H_2O_2 (Fig. 5(b)). For the CV curve measurements, 100 mM glucose was provided under air state. According to Fig. 5(b), the onset potential of HPRR by cascade reaction was observed at 0.8 V vs. Ag/AgCl, and the current showing the reactivity of cascade reaction was 68.7 μA at 0.3 V vs. Ag/AgCl. Namely, the current produced by cascade reaction was 89% of that measured in 3 mM H_2O_2. Conclusively, when 100 mM glucose that is the same concentration to anodic fuel was injected, desirable cascade reaction occurred properly with the help of GF/HRP/GOx/Gelatin-GA without separate injection of H_2O_2 for promoting the reactivity of HPRR.

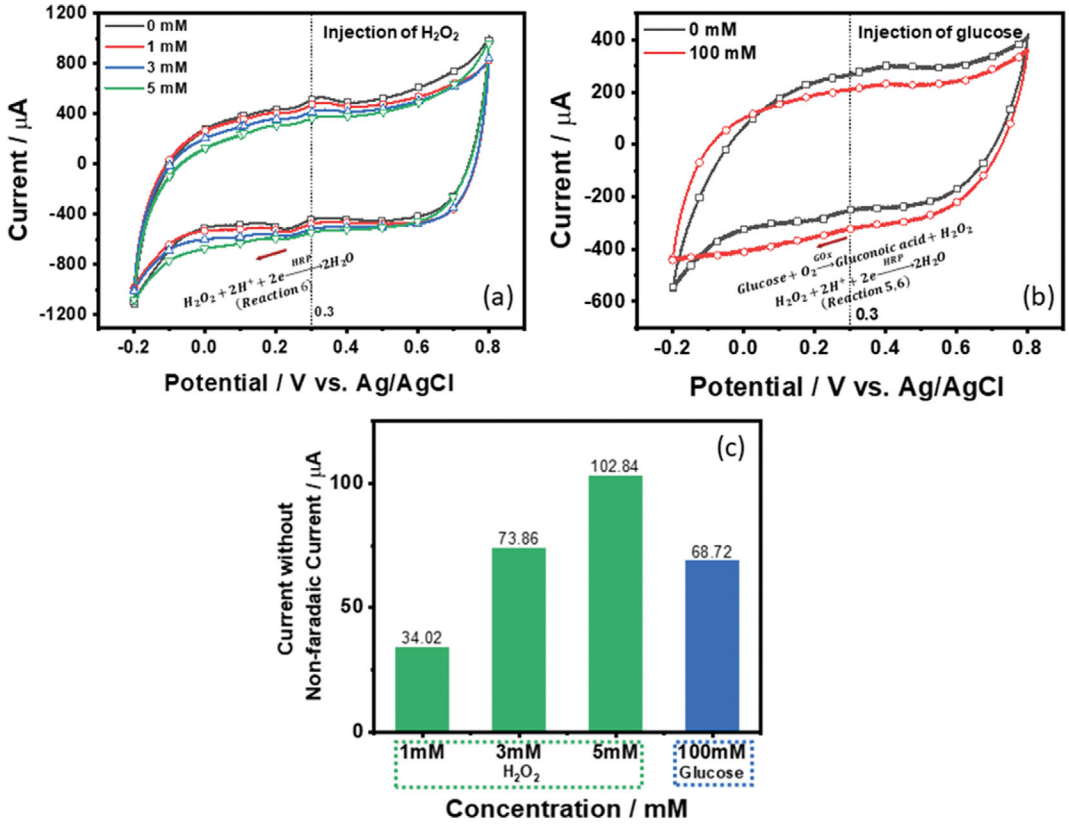

Fig. 5. CV curves showing (a) the reactivity of hydrogen peroxide reduction reaction (HPRR) measured by the injection of 0, 1, 3, and 5 mM H_2O_2 with GF/HRP/Gelatin-GA cathode at air state and (b) the reactivity of cascade reaction measured by the injection of 0 and 100 mM glucose with GF/HRP/GOx/Gelatin-GA cathode at air state. (c) Comparison of current density measured at 0.3 V vs. Ag/AgCl.

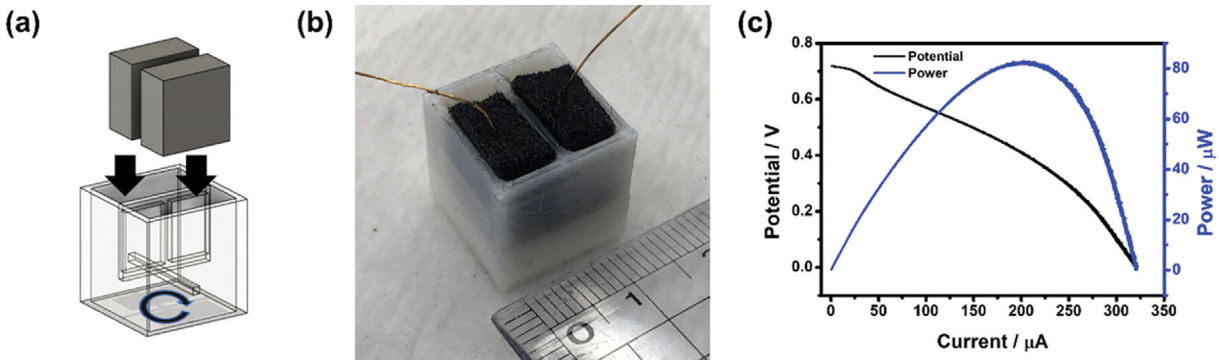

Fig. 6. (a) Design and (b) photo image of in-house mini-sized EBFC kit, and (c) polarization curve of EBFC full cell using GF/TTF/GOx/Gelatin-GA and GF/HRP/GOx/Gelatin-GA as anode and cathode. For the tests, 0.1 M SAB (pH 5.2) containing 100 mM glucose was used as electrolyte, and the potential scan rate was 10 mV/s in air state.

3. Performance Evaluations of EBFC Full Cells

Polarization curves were measured to evaluate the performance of EBFC full cells using optimally designed anodes and cathodes. Regarding the design of EBFC kit, an in-house mini-sized EBFC kit was fabricated (Fig. 6). More specifically, magnetic stirring space was included at the bottom part of the kit to form fluid flow. With the space, hydrogen ions produced in anode can be quickly transferred to cathode, while the size of the EBFC kit is 1.5×1.5×1.5 cm^3 (Fig. 6(b)). Two 1×1 cm^2 GF electrodes corresponding to anode and cathode, and 3 mL electrolyte are further included.

According to the polarization curve of EBFC full cell (Fig. 6(c)), its open circuit voltage (OCV) was 0.71 V, while its theoretical OCV corresponded to the difference in onset potentials between GOR (anodic reaction) and HPRR (cathodic reaction) is ~0.7 V (see Figs. 4(b) and 5(b)). This means that actual OCV of EBFC full cell is very close to its theoretical OCV, implying that overpotentials of both anodic and cathodic reactions are very low. In terms of maximum power density, this EBFC full cell produced 82 μW at 0.37 V vs. Ag/AgCl. Practically, this is enough electricity to drive small-sized implanted devices because it is known that power required for driving the implanted devices is ~50 W level. This indicates that mini-sized EBFC can generate the proper amount of electricity to drive small sized implanted devices.

CONCLUSION

New membraneless EBFCs were established. For further enhancing the performance of membraneless EBFCs, new 3D-GF electrodes were developed. With the newly developed 3D-GF electrode, the amount of loaded catalytic components was increased, while the reactivity of redox reactions required for operation of membraneless EBFCs was enhanced. For actually driven membraneless EBFCs, anodic catalyst including GOx and TFT mediator, and a cascade structure containing HRP and GOx was considered as cathodic catalyst. To minimize leaching out of the enzyme molecules, gelatin crosslinked by GA was applied to both 3D electrodes. According to optical evaluations, both anodic and cathodic catalysts were evenly distributed onto 3D-GF electrodes, while anodic and cathodic currents of 103.5 and 68.7 μA were electrochemically measured at 0.3 V vs. Ag/AgCl. Finally, EBFC using such optimized catalytic structure showed a high power of 82 μW in a small size of 1.5×1.5×1.5 cm^3 with excellent design flexibility.

ACKNOWLEDGEMENTS

This study was supported by the Research Program funded by the SeoulTech (Seoul National University of Science and Technology).

REFERENCES

1. M. Mohammadi, M. Sedighi, R. Natarajan, S. H. A. Hassan and M. Ghasemi, *Korean J. Chem. Eng.*, **38**, 72 (2021).
2. O. Z. Sharaf and M. F. Orhan, *Renew. Sustain. Energy Rev.*, **32**, 810 (2014).
3. S. Cosnier, A. J. Gross, F. Giroud and M. Holzinger, *Curr. Opin. Electrochem.*, **12**, 148 (2018).
4. J. Lee, J. Ji, K. Hyun, H. Lee and Y. Kwon, *Sensors Actuators B Chem.*, **372**, 132647 (2022).
5. J. Lee, K. Hyun and Y. Kwon, *J. Ind. Eng. Chem.*, **93**, 383 (2021).
6. B. Bhargawa, Y. Xu, I. K. Yoo, S. G. Kang and K. Ryu, *Korean J. Chem. Eng.*, **39**, 3048 (2022).
7. N. Hossain, L. L. Hoong, P. Barua, M. E. M. Soudagar and T. M. I. Mahlia, *Korean J. Chem. Eng.*, **38**, 2493 (2021).
8. S. El Ichi-Ribault, J. P. Alcaraz, F. Boucher, B. Boutaud, R. Dalmolin, J. Boutonnat, P. Cinquin, A. Zebda and D. K. Martin, *Electrochim. Acta*, **269**, 360 (2018).
9. A. Niiyama, K. Murata, Y. Shigemori, A. Zebda and S. Tsujimura, *J. Power Sources*, **427**, 49 (2019).
10. X. Wang, J. H. Kim, Y. B. Choi, H. H. Kim and C. J. Kim, *Korean J. Chem. Eng.*, **36**, 1172 (2019).
11. M. Kizling, M. Dzwonek, A. Nowak, Ł. Tymecki, K. Stolarczyk, A. Więckowska and R. Bilewicz, *Nanomaterials*, **10**, 1 (2020).
12. M. Christwardana, Y. Chung and Y. Kwon, *Korean J. Chem. Eng.*, **34**, 3009 (2017).
13. Y. Chung, Y. Ahn, D. H. Kim and Y. Kwon, *J. Power Sources*, **337**, 152 (2017).
14. Y. Chung, M. Christwardana, D. C. Tannia, K. J. Kim and Y. Kwon, *J. Power Sources*, **360**, 172 (2017).
15. L. Wang, X. Wu, B. S. Q. Su, R. Song, J.-R. Zhang and J.-J. Zhu, *Adv. Energy Sustain. Res.*, **2**, 2100031 (2021).
16. P. N. Bartlett and F. A. Al-Lolage, *J. Electroanal. Chem.*, **819**, 26 (2018).
17. J. Ji, S. Kim, Y. Chung and Y. Kwon, *J. Ind. Eng. Chem.*, **111**, 263 (2022).
18. A. Chaubey and B. D. Malhotra, *Biosens. Bioelectron.*, **17**, 441 (2002).
19. K. Hyun, S. Kang, J. Kim and Y. Kwon, *ACS Appl. Mater. Interfaces*, **12**, 23635 (2020).
20. M. N. Zafar, N. Beden, D. Leech, C. Sygmund, R. Ludwig and L. Gorton, *Anal. Bioanal. Chem.*, **402**, 2069 (2012).
21. C. Bunte, L. Hussein and G. A. Urban, *J. Power Sources*, **247**, 579 (2014).
22. K. Hyun, J. Lee, S. Kang and Y. Kwon, *J. Energy Chem.*, **61**, 155 (2021).
23. J. Lee, K. Hyun, J. M. Park, H. S. Park and Y. Kwon, *Int. J. Energy Res.*, **45**, 20959 (2021).
24. Y. Lin, M. Bariya, H. Y. Y. Nyein, L. Kivimäki, S. Uusitalo, E. Jansson, W. Ji, Z. Yuan, T. Happonen, C. Liedert, J. Hiltunen, Z. Fan and A. Javey, *Adv. Funct. Mater.*, **29**, 1 (2019).
25. R. Zumpano, L. Lambertini, C. Tortolini, P. Bollella, G. Favero, R. Antiochia and F. Mazzei, *J. Power Sources*, **476**, 228615 (2020).
26. K. Haneda, S. Yoshino, T. Ofuji, T. Miyake and M. Nishizawa, *Electrochim. Acta*, **82**, 175 (2012).
27. S. Kang, K. S. Yoo, Y. Chung and Y. Kwon, *J. Ind. Eng. Chem.*, **62**, 329 (2018).
28. G. Li, Z. Li, C. Xu, Z. Hou and Z. Hu, *ChemElectroChem*, **8**, 4529 (2021).
29. U. Salaj-Kosla, S. Pöller, Y. Beyl, M. D. Scanlon, S. Beloshapkin, S. Shleev, W. Schuhmann and E. Magner, *Electrochem. Commun.*, **16**, 92 (2012).
30. S. C. Barton, M. Pickard, R. Vazquez-Duhalt and A. Heller, *Biosens. Bioelectron.*, **17**, 1071 (2002).
31. H. An, H. Jeon, J. Ji, Y. Kwon and Y. Chung, *J. Energy Chem.*, **58**,

463 (2021).
32. J. Ji, S. Ro and Y. Kwon, *J. Ind. Eng. Chem*., **87**, 242 (2020).
33. J. Ji, J. Woo, Y. Chung, S. H. Joo and Y. Kwon, *Appl. Surf. Sci*., **511**, 145449 (2020).
34. J. Luo, L. Ma, F. Svec, T. Tan, Y. Lv, K. Chansaenpak, A. Kamkaew, S. Lisnund, P. Prachai, P. Ratwirunkit, T. Jingpho, V. Blay and P. Pinyou, *Biotechnol. J*., **11**, 1 (2021).
35. K. Elouarzaki, M. Bourourou, M. Holzinger, A. Le Goff, R. S. Marks and S. Cosnier, *Energy Environ. Sci*., **8**, 2069 (2015).
36. J. Ji, Y. Chung, K. Hyun, K. Y. Chung and Y. Kwon, *J. Ind. Eng. Chem*., **88**, 366 (2020).
37. A. Haeberlin, A. Zurbuchen, J. Schaerer, J. Wagner, S. Walpen, C. Huber, H. Haeberlin, J. Fuhrer and R. Vogel, *Europace*, **16**, 1534 (2014).
38. R. Hinchet, H. J. Yoon, H. Ryu, M. K. Kim, E. K. Choi, D. S. Kim and S. W. Kim, *Science* (80-.), **365**, 491 (2019).
39. M. Christwardana, Y. Chung, D. H. Kim and Y. Kwon, *J. Ind. Eng. Chem*., **71**, 435 (2019).
40. M. J. González-Guerrero, F. J. del Campo, J. P. Esquivel, F. Giroud, S. D. Minteer and N. Sabaté, *J. Power Sources*, **326**, 410 (2016).